Muon-spin-rotation studies of the temperature dependence of the magnetic penetration depth in the $YBa_2Cu_3O_x$ family and related compounds

P. Zimmermann, H. Keller, S. L. Lee,* I. M. Savić, M. Warden, and D. Zech
Physik-Institut der Universität Zürich, CH-8057 Zürich, Switzerland

R. Cubitt
Institut Max von Laue-Paul Langevin, 38042 Grenoble, Cedex, France

E. M. Forgan
School of Physics and Space Research, University of Birmingham, Birmingham B15 2TT, United Kingdom

E. Kaldis, J. Karpinski, and C. Krüger
Laboratorium für Festkörperphysik ETH, CH-8093 Zürich, Switzerland

(Received 23 January 1995)

A systematic muon-spin-rotation (μ^+SR) study is presented of the temperature dependence of the London penetration depth in sintered powder samples of the $YBa_2Cu_3O_x$ system and related compounds. The in-plane penetration depth λ_{ab} is estimated from the μ^+SR depolarization rate of $Bi_2Sr_2CaCu_2O_{8+\delta}$, $YBa_2Cu_4O_8$, and a series of samples of the $YBa_2Cu_3O_x$ family, respectively. It is found that not only the low-temperature value $\lambda_{ab}(0)$, but also the temperature behavior $\lambda_{ab}(T)$ is specific to each compound. The form of $\lambda_{ab}(T)$ can be well characterized by a simple power law. In particular, the $YBa_2Cu_3O_x$ family shows a systematic variation of the form of $\lambda_{ab}(T)$ with the oxygen content x which points to a varying coupling strength, whereas $\lambda_{ab}(0)$ as a function of x suggests a positive charge transfer into the CuO_2 planes with increasing oxygen doping. Furthermore, our data is consistent with an empirical ansatz which has been proposed in the framework of a Bose-gas picture of high-temperature superconductivity. As a consequence, the pressure and the isotope coefficients can be extracted from the μ^+SR depolarization rate and compared to direct measurements of these quantities, showing good agreement. Moreover, in the Bose-gas picture the variation of $\lambda_{ab}(T)$ in the $YBa_2Cu_3O_x$ family may be interpreted as a crossover from a dense (high-T_c) to a dilute (low-T_c) system of weakly interacting local pairs.

I. INTRODUCTION

The nature of the pairing mechanism of the CuO-based high-T_c systems is still an open question, although considerable progress in determining the unusual properties of these complex materials has been made. They are all highly anisotropic extreme type-II superconductors with very short coherence lengths. Furthermore, superconductivity depends sensitively on the carrier density in the CuO_2 planes, with the superconducting phase lying close to an antiferromagnetic phase. In addition, the normal state shows behavior unlike that of a normal metal. While most of the conventional superconductors are well described by the weak-coupling BCS theory, the vast experimental data on the high-T_c superconductors are not in every aspect consistent with this theory. For instance, there are measurements indicating that the cuprates could be in the strong-coupling limit with gap to T_c ratio $2\Delta_0/k_BT_c \approx 5-8$, see, e.g., Ref. 1 for a review and Ref. 2 for recent experimental work. As a consequence many new models have been proposed in recent years[3] in an attempt to present a pairing mechanism which would explain those unconventional properties.

Although the theoretical and experimental situation in the field of high-T_c superconductivity seems to be far from being clarified, these systems nevertheless show common trends in the relations between certain parameters. In particular, Uemura *et al.*[4–6] found a remarkable relationship between T_c and the zero-temperature μ^+SR relaxation rate $\sigma(0) \propto n_s/m^*_{ab}$ (with n_s the superconducting carrier density and m^*_{ab} the in-plane effective mass), which holds for many of the cuprate families. This "universal" behavior can be obtained from a simple scaling ansatz and the assumption that high-T_c superconductors belong to the three-dimensional (3D)-xy universality class.[7] Moreover, this ansatz implies important consequences for the pressure and the isotope effect, two crucial parameters of superconductivity, and also provides constraints for a microscopic theory.[7–9]

In order to help elucidate the issues raised above, a detailed and systematic study of the normal and superconducting properties of various high-T_c systems is required. The muon-spin-rotation (μ^+SR) technique has already made important contributions in this field. As an experimental method μ^+SR is unique because the positive muon acts as a microscopic probe of local magnetic fields in the bulk of a sample. By performing μ^+SR in the mixed state of a superconductor one is able to extract the internal field distribution, which reflects the given vortex structure. It is therefore possible to investigate directly

the complex vortex structures and dynamics of the cuprate high-T_c superconductors on a microscopic scale, see, e.g., Refs. 10–13 for recent work. Moreover, the magnetic penetration depth λ, one of the fundamental lengths of a type-II superconductor, can be determined from the measured local magnetic-field distribution. Since λ is related to the superconducting order parameter, the temperature dependence of λ provides direct informations on the pairing state, see, e.g., Refs. 14–18 for recent work.

In the following, systematic μ^+SR experiments on sintered $YBa_2Cu_3O_x$(Y123), $YBa_2Cu_4O_8$ (Y124), and $Bi_2Sr_2CaCu_2O_{8+\delta}$ (Bi2212) samples are presented. Section II explains the principles of the μ^+SR technique and its application in the mixed state of a superconductor. The estimation of the in-plane penetration depth λ_{ab} in terms of the μ^+SR depolarization rate is discussed. Measurements of the temperature dependence of λ_{ab} for the various compounds are described in Sec. III. It is shown that not only the low-temperature value $\lambda_{ab}(0)$, but also the whole temperature dependence of λ_{ab}, is characteristic of each compound and, in the Y123 family, varies in a systematic way with the oxygen stoichiometry x. The possible reasons for this are discussed in Sec. IV. Since our data is in good agreement with the empirical ansatz proposed by Schneider and Keller,[7] the values of the pressure and the isotope effect are calculated from the depolarization rates and compared to directly measured values of these quantities. In addition, the Bose-gas picture which leads to this ansatz can also account for the varying shape of $\lambda_{ab}(T)$. In Sec. V we summarize our results and conclusions of this study. The recent results presented here complement earlier preliminary measurements on these materials.[19–21]

II. μ^+SR IN THE MIXED STATE

The application of the μ^+SR technique in the mixed state of a superconductor can, in principle, measure the internal microscopic field distribution. As a consequence it is possible to extract the magnetic penetration depth λ, one of the fundamental lengths in superconductivity. In a μ^+SR experiment (more precisely: transverse field μ^+SR) highly spin-polarized positive muons are implanted into the sample, which is situated in an applied magnetic field perpendicular to the initial direction of the muon spins. During a short thermalization process ($<10^{-10}$ s) the muons come to rest at an interstitial site without losing their polarization. Each muon then undergoes Larmor precession in the local magnetic field $\mathbf{B}_\mu$ at the muon site with a frequency $\omega=\gamma_\mu B_\mu$, where $\gamma_\mu=2\pi\times 135.5$ MHz/T is the gyromagnetic ratio of the muon. After a mean lifetime of 2.2 μs the muon decays into a positron and two neutrinos. Because of parity violation the decay positron is preferentially emitted in the direction of the muon spin. This allows one to monitor the time evolution of the muon polarization by registering the decay events and the corresponding muon lifetime. To this end, each incoming muon starts a clock while the decay event stops it. Counting the number of events as a function of the time between start and stop of the clock yields the μ^+SR time histogram, which can generally be written in the following form:[22]

$$N(t)=N_0\exp(-t/\tau_\mu)[1+AP(t)]+b \ . \tag{1}$$

Here N_0 is a normalization constant, τ_μ the mean lifetime of the muon, A the maximum experimental decay asymmetry (precession amplitude), $P(t)$ is the muon-spin polarization, and b is a time-independent, uncorrelated background. Choosing the initial muon-spin direction parallel to the x axis, the time-dependent polarization in Eq. (1) in the simple case of a homogeneous field $\mathbf{B}$ pointing in an arbitrary direction is[23]

$$P_x(t)=P_x(0)\frac{B_y^2+B_z^2}{B^2}\cos(\gamma_\mu Bt) \ . \tag{2}$$

In the mixed state of a superconductor there exist spatially varying fields which are described by a probability distribution $p(\mathbf{B})$. The resulting polarization is then given by

$$P_x(t)=P_x(0)\int\frac{B_y^2+B_z^2}{B^2}\cos(\gamma_\mu Bt)p(\mathbf{B})d^3\mathbf{B} \ . \tag{3}$$

The precession signal $P_x(t)$ is therefore damped. In a transverse-field geometry (fields perpendicular to the x axis), the damping can be expressed in terms of a relaxation function $R(t)$:

$$P_x(t)=R(t)\cos(\gamma_\mu\langle B\rangle t) \ , \tag{4}$$

with $\langle B\rangle$ the first moment of $p(\mathbf{B})$. In the simple case of a Gaussian distribution, the relaxation function takes the form

$$R(t)=\exp(-\sigma^2t^2) \ . \tag{5}$$

The quantity σ is the muon-spin depolarization rate which is related to the second moment $\langle\Delta B^2\rangle$ of the field distribution $p(\mathbf{B})$ according to

$$\langle\Delta B^2\rangle=2\sigma^2/\gamma_\mu \ . \tag{6}$$

In the mixed state of a type-II superconductor the probability distribution $p(\mathbf{B})$ is given by the spatially varying fields from the vortex lattice and therefore depends on the magnetic penetration depth. The general expression for the zero-temperature limit of λ for an isotropic superconductor is given as[24]

$$1/\lambda^2(0)=[1+\xi/l]^{-1}\mu_0e^2n_s(0)/m^* \ , \tag{7}$$

where ξ is the coherence length and l the electron mean-free path. Because the coherence length is extremely small in the cuprate superconductors, these systems are in the clean limit[6] ($\xi/l\ll 1$), so that λ can be approximated by the London penetration depth λ_L:

$$1/\lambda^2(0)\simeq 1/\lambda_L^2(0)=\mu_0e^2n_s(0)/m^* \ . \tag{8}$$

The field distribution of extreme type-II superconductors was calculated using the London theory approach ($B_a<B_{c2}/4$) in the case of a triangular lattice,[25,26] leading to a relation between the second moment $\langle\Delta B^2\rangle$ of $p(B)$ (width of the field distribution) and the magnetic penetration depth:

$$\langle \Delta B^2 \rangle = 0.00371 \Phi_0^2 \lambda^{-4} . \quad (9)$$

Equation (9) is only valid for applied fields $B_a > 2B_{c1}$, where $\langle \Delta B^2 \rangle$ is nearly independent of B_a. However, the cuprates are layered materials and therefore exhibit anisotropic behavior. This can be taken into account by introducing an effective-mass tensor which, in the uniaxial case has two eigenvalues m_{ab}^* and m_c^* for supercurrents flowing in the ab plane and along the crystallographic c axis, respectively. Then, Eq. (8) has the form

$$1/\lambda_{ab,c}^2 = \mu_0 e^2 n_s / m_{ab,c}^* . \quad (10)$$

As a result, the field distribution for the general situation, where the direction of $\mathbf{B}_a$ is arbitrary with respect to the crystallographic axes, is complex, also giving rise to local field components perpendicular to $\mathbf{B}_a$.[27,28] However, for $B_a \gg B_{c1}$ the local fields are nearly parallel to $\mathbf{B}_a$, causing the muon-spin depolarization to be determined only by the variation of the field component parallel to $\mathbf{B}_a$. For sintered polycrystalline samples one must take a proper average over all orientations of the crystal axes. In this respect it is convenient to define an effective penetration depth λ_{eff} by

$$\langle \Delta B^2 \rangle_{\text{sintered}} = 0.00371 \Phi_0^2 \lambda_{\text{eff}}^{-4} , \quad (11)$$

where $\langle \Delta B^2 \rangle_{\text{sintered}}$ is the second moment of the powder averaged field distribution. It was shown that λ_{eff} is solely determined by λ_{ab} if the effective mass ratio $(m_c^*/m_{ab}^*)^{1/2} = \lambda_c/\lambda_{ab} \gtrsim 5$.[29,26,30] Analyzing μ^+SR data of sintered samples reveals that to a good approximation the relaxation function $R(t)$ is given by the Gaussian of Eq. (5). For practical use λ_{ab} can therefore be extracted directly from the muon-depolarization rate σ by using the simple relation:

$$\lambda_{ab}(\text{nm}) \simeq 224/\sqrt{\sigma(\mu\text{s}^{-1})} . \quad (12)$$

The derivation of λ_{ab} from the μ^+SR precession signal as given so far has been based on the assumption of a regular vortex lattice. Note that the muon needs only a short-range ordered flux lattice to sample the field distribution $p(B)$ of the ideal lattice. Although there is evidence for the existence of a vortex lattice at low temperature from neutron-scattering[31] and decoration experiments[32] the B-T phase diagram of the cuprates can be very complex and is not yet entirely understood.[33] In particular, pinning is generally present and leads to a distortion of the perfect flux lattice. The resulting disorder may considerably affect the ideal field distribution, leading to an additional broadening of $p(B)$ which can be taken into account by convolution of $p(B)$ with an appropriate broadening function.[25,34] However, the applied fields used in transverse field μ^+SR are much higher than B_{c1}, so the penetration depth $\lambda \propto B_{c1}^{-1/2}$ is larger than the intervortex distance $d \propto \langle B \rangle^{-1/2}$. In this case the intervortex forces responsible for the regular arrangement may dominate the pinning forces, leading to a vortex structure which still exhibits short-range order. On the other hand, random pinning in cuprate systems having extremely high anisotropy (with quasi-2D vortex structure) introduces field variations along the $\mathbf{B}$ direction and may reduce the second moment $\langle \Delta B^2 \rangle$ below the value of the ideal lattice given by Eq. (9).[35] This is possible if pinning prevents interlayer alignment of the pancake vortices leading to partial destructive interference of the field modulation in different layers. Unusually narrow field distributions measured using μ^+SR have been attributed to this effect in highly anisotropic Bi2212 single crystals.[10,13] In addition to pinning, thermal fluctuations which destroy spatial correlations on the time scale of the muon lifetime may give rise to further deviations of $\langle \Delta B^2 \rangle$ from the ideal value, especially at high temperatures. It was shown[35] that the influence on $\langle \Delta B^2 \rangle$ of thermal (dynamic) vortex fluctuations is qualitatively similar to the effects of pinning induced (static) vortex disorder. Experimental evidence for a significant influence of thermal fluctuations on the linewidth of $p(B)$ have recently been obtained.[36]

According to the discussion above, the extraction of a reliable value for the penetration depth from the measured field distribution using μ^+SR may be difficult because pinning, thermal fluctuations, as well as demagnetization effects give rise to a distorted vortex lattice. However, if one is mainly interested in the second moment of $p(B)$ and not in the specific line shape, it was shown[22] that in sintered samples the assumption of a Gaussian form of $p(B)$ is valid and yields reasonable estimates of λ_{ab} which compare well with those obtained with other experimental techniques. One has to bear in mind that a misinterpretation in $\langle \Delta B^2 \rangle$ of say 25% results in a change of the estimated λ_{ab} by only 7% [Eq. (12)], which is of the order of the experimental error. For example, an evaluation of λ_{ab} in $YBa_2Cu_3O_{7-\delta}$, taking into account the critical-state model and broadening by pinning,[34] yields a value of $\lambda_{ab}(0) = 130(10)$ nm, in excellent agreement with Ref. 22. Moreover, a detailed μ^+SR study of the magnetic penetration depth in various sintered samples of the $(BiPb)_2Sr_2(CaY)Cu_2O_{8+\delta}$ family was performed, where all possible effects which influence the field distribution were taken into account in the data analysis.[14] Nevertheless, the values of λ_{ab} the authors obtained from this extensive analysis compare quite well with those determined from the same data by using a simple Gaussian relaxation function (for comparison see also Refs. 4 and 6). Analyzing μ^+SR data in terms of the depolarization rate σ is therefore a useful and straightforward method for estimating the penetration depth and for systematic investigations of this important parameter of superconductivity in various cuprate families.

III. EXPERIMENTAL RESULTS

The samples used in this study were sintered disks of high quality with diameters between 10 and 25 mm. All samples of the Y123 family[37] and the Y124 sample[38] were prepared at the ETH Zurich (Switzerland), the Bi2212 disk at IBM Zurich. Characterization was performed by superconducting quantum interference device magnetization, dc resistivity measurements, and x-ray diffractometry, respectively. The determination of the oxygen content in the Y123 samples is described elsewhere.[39] A summary of the characterization results is

given in Table I. It lists T_c (onset of superconductivity as measured by dc magnetization) and the width of the transition ΔT_c (10–90 % magnetization) for all compounds. While ΔT_c of the highly oxygenated and the low oxygen samples are small, the samples with intermediate oxygen content $6.6 \leq x \leq 6.8$ exhibit a somewhat broader transition. Figure 1 shows T_c as a function of the oxygen content x of the Y123 samples. The two plateaus at 60 K for $x \lesssim 6.7$ and at 90 K for $x \gtrsim 6.9$ can clearly be distinguished. Note that the samples needed in μ^+SR have to be rather large compared to those used in other experimental techniques (say 10 mm in diameter and 2 mm in thickness). Therefore sintered samples are most appropriate for investigations which compare a large number of various superconductors from different cuprate families, since the quality of big single crystals is generally far less than that of sintered materials, apart from the difficulty of synthesizing many single crystals of different stoichiometry with comparable quality.

The experiments were performed at the Paul Scherrer Institut PSI (Switzerland) and some early experiments at TRIUMF (Canada). To achieve a transverse geometry, the low-momentum muons were spin rotated which has the advantage of focusing the muon beam on the target (the applied field is parallel to the muon momentum). Special attention was paid to ensure the same experimental setup for all samples, so that the measurement conditions were identical. In particular, it was assured that all muons stopped either in the sample or in the part of the sample holder made out of a plate of hematite (Fe_2O_3). Fe_2O_3 is an antiferromagnet wherein the muons see a local field of the order of 1.6 T. The corresponding spectral line does not interfere with the signal originating from the sample, leading to a spectrum nearly free of background. This has been demonstrated by performing zero-field-cooling measurements (see, e.g., Fig. 1 in Ref. 40 or Fig. 1 in Ref. 12, and Sec. II in Ref. 12 for explanation).

TABLE I. T_c (onset of magnetization) and ΔT_c (10–90 % magnetization) of all measured compounds. ΔT_c is a measure of the width of the superconducting transition and is seen to have higher values for $YBa_2Cu_3O_x$ with x between 6.6 and 6.8.

Sample	T_c(K)	ΔT_c(K)
$YBa_2Cu_3O_{6.970}$	91.3(5)	8
$YBa_2Cu_3O_{6.962}$	92.1(2)	7
$YBa_2Cu_3O_{6.955}$	91.8(5)	7
$YBa_2Cu_3O_{6.906}$	92.4(5)	11
$YBa_2Cu_3O_{6.828}$	88(1)	9
$YBa_2Cu_3O_{6.773}$	71.2(2)	16
$YBa_2Cu_3O_{6.702}$	69(1)	13
$YBa_2Cu_3O_{6.666}$	60.5(5)	17
$YBa_2Cu_3O_{6.602}$	59.4(4)	17
$YBa_2Cu_3O_{6.556}$	58.5(5)	8
$YBa_2Cu_3O_{6.546}$	59.4(5)	12
$YBa_2Cu_3O_{6.516}$	58.7(7)	12
$YBa_2Cu_4O_8$	82.0(5)	4
$Bi_2Sr_2CaCu_2O_{8+\delta}$	83.5(6)	18

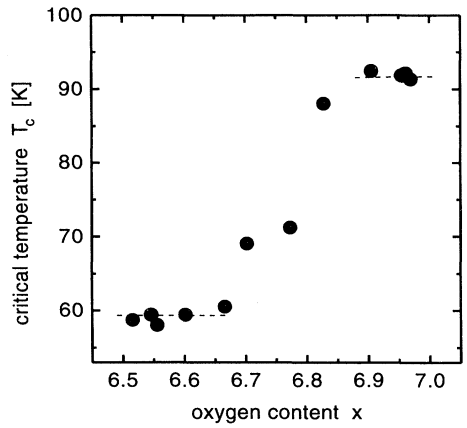

FIG. 1. Transition temperature T_c vs oxygen content x of the $YBa_2Cu_3O_x$ samples used in this study. Note the previously observed (Ref. 58) two plateaus at 60 and 90 K for $x \lesssim 6.7$ and $x \gtrsim 6.9$, respectively.

In order to apply Eq. (12) to estimate λ_{ab}, one must ensure that the applied field is high enough to justify the validity of Eq. (9). Therefore, the muon depolarization rate $\sigma \propto (\langle \Delta B^2 \rangle)^{1/2}$ was measured as a function of the applied field B_a at low temperatures, see Fig. 2. Note that this is not a field scan of σ, but each point in Fig. 2 represents a true field cooling. That is, the sample is slowly cooled from far above T_c to low temperatures in the corresponding field. It can be seen that all samples show a very similar behavior. The depolarization rate first increases with increasing field, then reaches a broad maximum and finally becomes constant above $B_a \simeq 150$ mT. For samples with a small value of σ at high fields

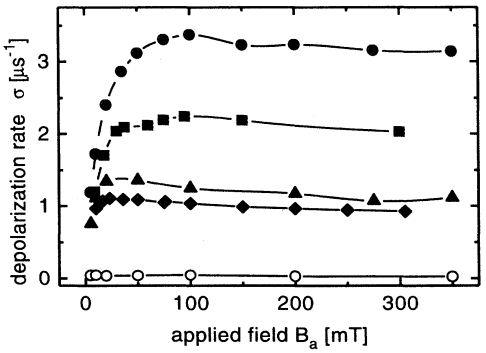

FIG. 2. Field dependence of the depolarization rate σ of various cuprate superconductors at 10 K (6 K for $YBa_2Cu_4O_8$). Note that σ becomes constant for applied fields above 150 mT. $\sigma(B_a)$ is plotted for $YBa_2Cu_3O_x$, $x=6.970$ (filled circles), $x=6.516$ (filled diamonds), $YBa_2Cu_4O_8$ (filled squares), and $Bi_2Sr_2CaCu_2O_{8+\delta}$ (filled triangles), respectively. Open circles denote σ measured far above T_c for $YBa_2Cu_3O_x$, $x=6.970$. In this case σ is field independent and of the same order in all the other samples (omitted for clarity). This small depolarization (about 0.1 μs^{-1}) most probably originates from copper nuclear moments.

(low oxygen Y123 and Bi2212) the maximum is at a field below 50 mT, while for the samples with larger σ (high oxygen Y123 and Y124) this maximum lies around 100 mT. The bump observed in $\sigma(B_a)$ can be explained by a distortion of the flux lattice due to nonlocal pinning,[41] since pinning leads to an enhancement of $\langle \Delta B^2 \rangle$ (Ref. 25) as stated in the previous section. This effect is most prominent at low fields near B_{c1}, where the intervortex forces are still small. According to Eq. (12), $\sigma \propto 1/\lambda_{ab}^2 \propto B_{c1}$ when the applied field is sufficiently high. Therefore, if one assumes that the applied field B_p at which $\sigma(B_a)$ takes a maximum is roughly equal to B_{c1}, then the high-field value of σ for each compound should scale with the corresponding B_p. This is in fair agreement with the data, see Fig. 3. Also shown in Fig. 2 is the constant and small σ measured at a temperature well above T_c. This depolarization most likely arises from nuclear copper moments. Our measurements of $\sigma(B_a)$ demonstrate that if $B_a > 150$ mT then for all samples the necessary condition for the existence of a more or less regular vortex lattice is achieved. The use of Eq. (12) is then a valid means of extracting λ_{ab}.

In a next step we measured the low-temperature depolarization rate at a field of 350 mT of the samples listed in Table I and, in addition the temperature dependence $\sigma(T)$ of a subset of these samples. The low temperature σ was used together with Eq. (12) to estimate $\lambda_{ab}(0)$. Table II presents the results, where $\sigma(0)$ is either the measured value of σ at low temperature or the value extrapolated to zero temperature from a fit to the temperature dependence of σ (see below). Note that these values are corrected by subtracting the part of the depolarization rate originating from the copper moments, which is of the order of 0.1 μs^{-1}, see Fig. 2. The errors of $\sigma(0)$ given in Table II are estimated experimental uncertainties; the statistical errors of the fit of the precession signal

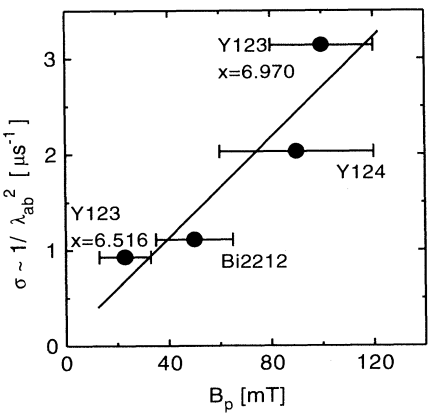

FIG. 3. Depolarization rate σ at high field (where $\sigma \propto \lambda_{ab}^{-2}$) plotted against the field B_p [where $\sigma(B_a)$ has a maximum] for the samples shown in Fig. 2. Y123 stands for $YBa_2Cu_3O_x$, Y124 for $YBa_2Cu_4O_8$, and Bi2212 for $Bi_2Sr_2CaCu_2O_{8+\delta}$, respectively. The errors are estimated by accounting for the uncertainty in determining B_p from the measured $\sigma(B_a)$ curve. Straight line is a linear fit to the data, see text.

TABLE II. Low-temperature depolarization rate $\sigma(0)$ and in-plane penetration depth $\lambda_{ab}(0)$ of the samples listed. The $\sigma(0)$ values were derived by fitting the temperature dependence of $\sigma(T)$, see text. The values marked by * represent direct measurements at low temperature. Also listed is the exponent n, a fit parameter of Eq. (13), which characterizes the form of the temperature dependence of λ_{ab}, see text.

Sample	$\sigma(0)(\mu s^{-1})$	$\lambda_{ab}(0)$(nm)	n
$YBa_2Cu_3O_{6.970}$	3.06(2)	130(10)	3.99
$YBa_2Cu_3O_{6.962}$	2.74(2)	135(10)	4.17
$YBa_2Cu_3O_{6.955}$	2.66(2)	140(10)	4.27
$YBa_2Cu_3O_{6.906}$	2.03(4)*	160(20)	
$YBa_2Cu_3O_{6.828}$	1.58(4)*	180(20)	
$YBa_2Cu_3O_{6.773}$	1.15(2)	210(15)	2.64
$YBa_2Cu_3O_{6.702}$	1.11(4)*	210(20)	
$YBa_2Cu_3O_{6.666}$	0.97(2)	225(15)	2.88
$YBa_2Cu_3O_{6.602}$	1.04(2)	220(15)	2.46
$YBa_2Cu_3O_{6.556}$	1.01(2)	225(15)	3.47
$YBa_2Cu_3O_{6.546}$	0.78(4)*	255(20)	
$YBa_2Cu_3O_{6.516}$	0.82(4)	250(20)	2.21
$YBa_2Cu_4O_8$	2.00(4)	160(20)	2.38
$Bi_2Sr_2CaCu_2O_{8+\delta}$	1.18(2)	205(15)	2.78

to Eq. (5) are much smaller. Our values for the penetration depth of Bi2212 and Y124 agree fairly well with other measurements, e.g., for Bi2212: 185(10) nm,[14] 240 nm,[5,6] (μ^+SR on sintered material), 180 nm,[13] (μ^+SR on single crystals), and 210 nm (Ref. 42) (magnetization on single crystals); for Y124: 174 nm (Ref. 43) (μ^+SR on sintered discs) and 196 nm (Ref. 44) (magnetization on grain-aligned powder). Some of the variation in the Bi2212 data may be due to slightly different oxygen deficiencies δ of the samples used in these studies. We note here that estimates of the penetration depth using the μ^+SR method are generally to be taken as lower limits because of the reasons already explained in the preceeding section.

Because Eq. (11) is valid for all $T < T_c$ the muon depolarization rate can also sample the temperature dependence of the penetration depth. We therefore measured σ as a function of temperature for a subset of the samples listed in Tables I and II. The results are presented in Figs. 4 and 5, where, for the sake of clarity the plots of $\sigma(T)$ of all the various samples are split into groups. Figures 4 and 5 show the normalized depolarization rate $\sigma(T)/\sigma(0) = \lambda_{ab}^2(0)/\lambda_{ab}^2(T)$ as a function of the reduced temperature T/T_c. In order to investigate and compare these data we characterize the overall temperature dependence of σ with an empirical power law of the form

$$\sigma(T) = \sigma(0)\left[1 - \left[\frac{T}{T_c}\right]^n\right] . \quad (13)$$

The solid lines in Figs. 4 and 5 represent the fits of each data set to Eq. (13). Note that for two specific values of the exponent n, Eq. (13) is actually the formula for $\lambda^{-2}(T)$ in the two-fluid model ($n = 4$) and in the model of the ideal charged Bose gas[45] ($n = 3/2$), respectively. The curve for $n = 3/2$ is added in Fig. 4(a) as a dashed line for comparison, as well as the dotted line, which depicts the

weak-coupling BCS case (taken from Ref. 46). The curve for the two-fluid model is omitted in Fig. 4 for clarity, because it would nearly coincide with the fit of the Y123 $x=6.970$ data (full circles). It is therefore shown as a dashed line in Fig. 5(b). The values of n extracted from our data are listed in Table II. It can be seen that the general feature of the measured $\sigma(T)$ is the weak or almost absent temperature dependence for $T/T_c<0.3$ followed by an increasingly stronger T dependence for increasing T/T_c. The curvature at intermediate temperatures and the slope of the nearly linear part below T_c are typical for each sample. Therefore Eq. (13) describes the data well, especially the curvature at intermediate temperatures, which is the part where the data of the various samples differ most significantly.

Furthermore, Figs. 4 and 5 show clearly a systematic trend towards flatter behavior of $\sigma(T)/\sigma(0)$ with decreasing oxygen content x in the Y123 family, the notable exception of the Y123 $x=6.556$ sample with $n=3.47$ notwithstanding. Only the members with x above 6.9 show a temperature dependence similar to the two-fluid model. The behavior of $\sigma(T)/\sigma(0)$ of Y124 with $n=2.38$ [Fig. 5(b), open circles] and Bi2212 with $n=2.78$ [Fig. 5(b), full circles] also differs from the well oxygenated Y123. We note however, that there are small deviations from Eq. (13) in the vicinity of T_c, which probably can be attributed to thermal fluctuations. In addition, the dimensions of the vortex core near T_c can no longer be ignored, because the coherence length diverges at the transition. As a consequence, the simple relation between the penetration depth and the width of the field distribution is no longer valid, since Eq. (9) is based on London theory. The data of Y123 $x=6.516$ [Fig. 4(b), full triangles] exhibits some scatter over the whole temperature range, so the exponent $n=2.21$ can only be regarded as an approximate value. A further complication concerns the Bi2212 data. If $\sigma(T)$ is assessed over the whole temperature range one has to be aware that temperature-dependent changes in the vortex structure may influence the results, as discussed in Sec. II. In the range of applied fields used in this work (a few tenths of a Telsa) the possible change in the vortex structure as suggested by the irreversibility line takes place only very near T_c in Y123 (Ref. 47) and Y124,[48] respectively. However, due to the extremely high anisotropy of the Bi2212 com-

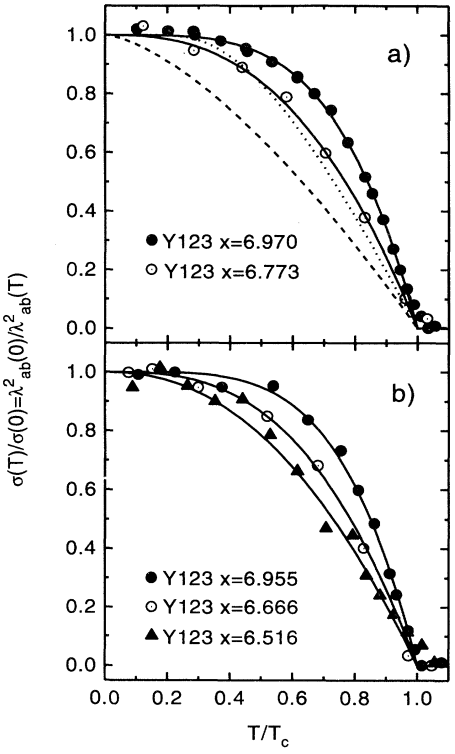

FIG. 4. Normalized depolarization rate $\sigma(T)/\sigma(0)$ as a function of the reduced temperature T/T_c at 350 mT:(a) $YBa_2Cu_3O_x$ (Y123) with oxygen content $x=6.970$ (full circles) (taken from Ref. 22); Y123, $x=6.773$ (open circles). (b) Y123, $x=6.955$ (full circles); Y123, $x=6.666$ (open circles); Y123, $x=6.516$ (full triangles). The solid lines are fits to Eq. (13) with the exponent n ranging from 2.21 (Y123, $x=6.516$) to 4.27 (Y123, $x=6.955$). For comparison, the dotted line shows the weak coupling BCS prediction, while the dashed line represents the case of the ideal charged Bose gas with $n=3/2$. The two-fluid model ($n=4$) is omitted, because it would almost coincide with the fit for Y123, $x=6.970$.

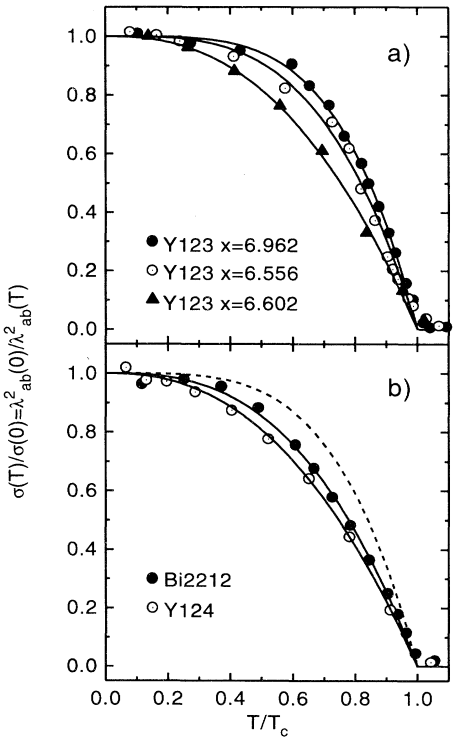

FIG. 5. Normalized depolarization rate $\sigma(T)/\sigma(0)$ as a function of the reduced temperature T/T_c at 350 mT:(a) $YBa_2Cu_3O_x$ (Y123) with oxygen content $x=6.962$ (full circles); Y123, $x=6.602$ (full triangles); Y123, $x=6.556$ (open circles). (b) $Bi_2Sr_2CaCu_2O_{8+\delta}$ (Bi2212) (full circles); $YBa_2Cu_4O_8$ (Y124) (open circles). The solid lines are fits to Eq. (13). For comparison, the dashed line in (b) corresponds to the two-fluid model (exponent $n=4$).

pound thermal fluctuations already become prominent at temperatures well below T_c. As shown in Ref. 13 the field distribution at low temperatures is still similar to that of a 3D flux-line lattice, and the μ^+SR depolarization rate provides a reasonable estimate of $\lambda_{ab}(0)$. At elevated temperatures and in particular above the melting transition, the assumptions leading to Eq. (12) are no longer valid. The interpretation of $\sigma(T)$ of Bi2212 in terms of the in-plane penetration depth is then only possible at low temperatures. At the melting transition a rather sharp change in $\sigma(T)$ is seen in single-crystal measurements.[13] Such a feature is not observed in the sintered Bi2212 data, see Fig. 5(b), where it should appear at $T/T_c \approx 0.35$. The reason for this may be the dependence of the melting transition on the angle between the applied field and the crystallographic c axis. Any sharp changes in $\sigma(T)$ could be smeared out in a sintered sample because of the isotropically distributed orientations of the crystallites. As a closing remark we point to the fact that measurements on single crystals generally show much flatter temperature dependence than corresponding sintered samples, e.g., small-angle neutron-scattering,[49] microwave and μ^+SR work on 90 K Y123,[50] and μ^+SR (Ref. 11) on Bi2212. In μ^+SR this phenomenon is partly due to smaller $\sigma(0)$ in single crystals, the origin of which is still not understood completely. This problem is assessed in Ref. 11, where the authors state that in the case of Bi2212 one of the reasons may be not fully or inhomogeneously oxygenated crystals.

IV. DISCUSSION

A. Carrier doping and systematic trends

According to Eq. (8) the penetration depth is related to the superconducting carrier density which in turn is determined by the order parameter. Therefore, the temperature dependence of the magnetic penetration depth is one of the most important properties concerning information on the pairing state. Assessing $\lambda(T)$ in the intermediate temperature range yields informations about the coupling strength, while measurements at low temperatures could in principle probe the symmetry of the pairing state. Any theory of superconductivity should be able to predict the temperature behavior of λ. However, the situation is much more complicated due to various experimental constraints imposed on these measurements (e.g., techniques which probe only the surface of a sample).

In the case of Y123 Nicol and Carbotte[51] have shown that the temperature dependence of the $YBa_2Cu_3O_{6.970}$ sample is consistent with the prediction of a phenomenological, marginal-Fermi-liquid model with a superconducting gap to T_c ratio of $2\Delta_0/k_BT_c \simeq 5$, suggesting strong coupling. The two-fluid model would also well describe $\sigma(T)$ of this highly oxygenated sample, see Fig. 4(a). The coupling strength influences the form of $\lambda_{ab}(T)$; a decreasing value of the coupling strength tends to flatten $\lambda_{ab}^{-2}(T)$.[52–54] Depending on the parameters of the respective model, calculations of $\lambda_{ab}^{-2}(T)$ can even lie above the two-fluid model if the coupling is chosen sufficiently strong.[51,54]

Similar features are seen in Figs. 4 and 5 and Table II: First, the data points of Y123 with $x=6.962$ and $x=6.955$ lie above the two-fluid curve; fits to Eq. (13) yield exponents $n=4.17$ and $n=4.27$, respectively. Therefore, our results of Y123 with high oxygen content seem to point toward strong coupling. This is supported by recent work of Reeves[55] (specific heat) and Neminsky and Nikolaev[56] (ac susceptibility). Second, the temperature behavior of σ in low oxygenated Y123, the Y124, and Bi2212 samples are not consistent with the two-fluid model. In particular, there is a trend in $\sigma(T)$ of the Y123 family towards flatter temperature dependence with decreasing oxygen content x. The exponent n ranging from 4.27 for $x=6.955$ to 2.21 for $x=6.516$ reflects this trend, indicating a decreasing coupling strength with reduced oxygen content. $\sigma(T)$ of the highly oxygen-deficient samples with small n can also be described fairly well by weak-coupling BCS theory ($2\Delta_0/k_BT_c=3.52$), because the BCS curve shown in Fig. 4(a) is similar to Eq. (13) with $n \simeq 2.4$.

The theoretical calculations presented in Ref. 54 could give an alternative explanation of this trend in the Y123 family. There it is shown that in the framework of the complete anisotropic Eliashberg equations an increasing anisotropy in the pairing also flattens $\lambda_{ab}^{-2}(T)$. However, the amount of change in the form of $\lambda_{ab}^{-2}(T)$ depends on the coupling strength. Taking a value representative for strong coupling, the dependence of $\lambda_{ab}^{-2}(T)$ on the pairing anisotropy is greatly reduced. In this case, all the curves calculated for various values of the pairing anisotropy come close to the two-fluid behavior.[54] Therefore, it is unlikely that the observed variation of the temperature dependence of the in-plane penetration depth as extracted from the depolarization rate in Y123 is due to an increasing pairing anisotropy with decreasing x.

Systematic trends in the Y123 family are also manifest in the low-temperature values of the measured depolarization rate. The dependence of $\sigma(0)$ and $\lambda_{ab}(0)$ on oxygen stoichiometry x is shown in Figs. 6(a) and 6(b), respectively. It is clearly seen that $\lambda_{ab}(0)$ is decreasing with increasing x, ranging from 255(20) nm for low x to 130(10) nm for high x. These results agree well with magnetic torque measurements of $\lambda_{ab}(0)$ by Janossy *et al.*[57] The stoichiometry dependence is stronger above $x=6.8$, while below this value $\lambda_{ab}(0)$ is only weakly dependent on the oxygen content, notwithstanding the scatter in the data for very low x. Because $\sigma \propto \lambda^{-2}$ these features are also present somewhat more pronounced in $\sigma(x)$, see Fig. 6(a). Comparing $\sigma(x)$ with $T_c(x)$ (see Fig. 1) it can be seen that both data sets exhibit a plateau for low x. Also, the initial increase of $\sigma(x)$ roughly coincides with the region where T_c changes from 60 to 90 K. However, for $x>6.9$ the transition temperature T_c is almost independent of x, whereas σ is still increasing rather rapidly.

Since $\sigma \propto n_s/m_{ab}^*$, Fig. 6(a) implies that the superfluid density n_s/m_{ab}^* is monotonically increasing with oxygen content x. It was shown in Ref. 57 that the in-plane effective mass $m_{ab}^* \approx m_e$ for $x \simeq 7$ and it increases only to about $2m_e$ for $x \simeq 6.5$ (m_e is the electron mass). The

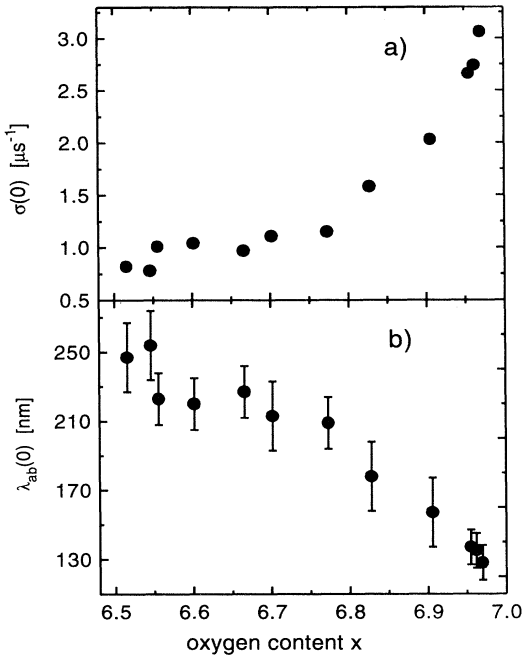

FIG. 6. Oxygen content dependence of (a), the low-temperature depolarization rate $\sigma(0)$ and (b), the estimations of $\lambda_{ab}(0)$ for the $YBa_2Cu_3O_x$ family. $\sigma(0)$ is monotonically increasing with increasing x, with $\sigma(0)$ nearly constant for $x<6.8$. The qualitative behavior of $\sigma(x)$ is similar to that of $T_c(x)$ except for $x>6.9$, see Fig. 1.

behavior of σ as a function of oxygen stoichiometry is therefore mainly determined by the superconducting carrier density n_s, suggesting a positive charge transfer from the CuO chains to the CuO_2 planes. Indeed, there are interesting similarities between $\sigma(x)$ and the bond-valence sum around the CuO_2 plane copper[58] which is related to the actual charge sitting on that particular copper atom. The nonlinear dependence of the zero-temperature depolarization rate on the oxygen stoichiometry reveals the complexity of the relation between the density of the carriers involved in superconductivity (pairs in the CuO_2 planes) and the number of holes in the whole Y123 system (given by the oxygen content x). Such a nontrivial relation is to be expected, since the pair density and therefore the superconducting properties (e.g., T_c) are correlated with structural parameters such as the crystallographic c axis,[37] plane-Cu to apex-O bond length[58] and oxygen ordering phenomena in the chains and the planes.[58,37,59]

In addition to $\lambda_{ab}(0)$, measurements of $\lambda_c(0)$ were also reported in Ref. 57. The results show that the anisotropy ratio $\gamma=\lambda_c/\lambda_{ab}=(m_c^*/m_{ab}^*)^{1/2}$ is increasing with decreasing oxygen content x. In that paper the authors interpret this behavior of γ in terms of the Lawrence-Doniach model of layered superconductors as due to a decreasing interlayer coupling strength. This is because $m_c^* \propto \lambda_c^2$ increases much more strongly with decreasing x than $m_{ab}^* \propto \lambda_{ab}^2$. The main contribution to the increase of γ is thus due to the interlayer carrier transport which is reduced with decreasing oxygen content. Since we observe a qualitative trend of $\sigma(T)$ becoming flatter with decreasing x, this may possibly reflect the increasing anisotropy in less than optimally doped Y123. This would imply that a comparatively small exponent n is an indication of a large anisotropy. According to Ref. 57 the values of γ range from 5 ($x\approx 7, n\approx 4$) to 25 ($x\approx 6.5, n\approx 2$). Interestingly, the structurally related compound Y124 lies between these limits, both for the exponent $n=2.38$, as well as for the anisotropy ratio $\gamma\approx 10$.[60]

The unconventional properties of the cuprate high-T_c superconductors have been the motivation to formulate models which propose mechanisms of superconductivity different from the electron-phonon interaction in the weak-coupling BCS theory. Some of these models lead to a d-wave-type pair-wave function. Considerable theoretical and experimental work has been done in this field, but the experimental results are still controversial, see, e.g., Ref. 61 for a short review and Ref. 62 for recent experiments. The measurements of $\sigma(T)$ presented here and interpreted in terms of $\lambda_{ab}^{-2}(T)$ do not allow to make definite statements about the pairing symmetry. To this end, precise measurements at very low temperatures could yield significant informations.

B. Generic properties

Recent μ^+SR studies of the magnetic penetration depth in various classes of cuprate superconductors revealed a remarkable empirical relation between T_c and the low-temperature limit of the depolarization rate $\sigma(0)\propto\lambda_{ab}^{-2}(0)\propto n_s(0)/m_{ab}^*$.[4-6] This relation seems to be universal for many cuprate high-T_c systems and other extreme type-II superconductors and, when plotted as T_c versus $\sigma(0)$ ("Uemura plot") exhibits the following features: (i) by increasing the carrier doping, T_c initially increases almost linearly, then saturates, and finally is suppressed for high carrier doping, (ii) the initial slope of the linear increase of $T_c(\sigma)$ appears to be nearly the same for different families, while the saturation and suppression of T_c starts at different values of $\sigma(0)$ for each family. According to Refs. 4 and 5 the relationship between T_c and $n_s(0)/m_{ab}^*$ points to rather strongly bound pairs, and therefore cannot be explained within the framework of weak-coupling BCS theory. Also, the pressure p and isotope mass m dependence of the transition temperature, described by the pressure coefficient

$$\alpha=\frac{d\ln T_c}{dp}\ , \tag{14}$$

and the isotope coefficient

$$\beta=-\frac{d\ln T_c}{d\ln m}=-\frac{m}{T_c}\frac{dT_c}{dm} \tag{15}$$

show generic behavior in several classes of doped cuprates.[7-9] Both $\alpha(T_c)$ and $\beta(T_c)$ have two nearly symmetric branches, one with positive and the other with negative values of the coefficients. These branches merge at T_c^m, the maximum T_c of the respective cuprate family.

The coefficients nearly vanish at T_c^m and their magnitude increases with decreasing T_c.

In order to account for these trends Schneider and Keller[7] originally proposed an empirical scaling ansatz for $T_c(\sigma)$ near the optimum stoichiometry of the form

$$\overline{T}_c = 2\overline{\sigma}(1-\overline{\sigma}/2) , \tag{16}$$

where $\overline{T}_c = T_c/T_c^m$ and $\overline{\sigma} = \sigma(0)/\sigma_m(0)$; $\sigma_m(0)$ is the depolarization rate of the optimally doped system. This ansatz can be justified by considering high-T_c systems as belonging to the 3D-xy universality class, being extreme type-II superconductors with short coherence length, uniaxial mass anisotropy, and complex order parameter. Note that the coherence lengths in the cuprates are comparable to their crystallographic lattice constants and that the coherence volume ξ^3 (size of a Cooper pair) is about 5 to 6 orders of magnitude smaller than in conventional BCS superconductors and therefore similar to that of ^{4}He. From this point of view high-T_c superconductivity may be discussed in terms of Bose condensation of weakly charged, interacting local pairs.[7] The μ^+SR data of a large number of cuprates indeed follow the ansatz given in Eq. (16). Moreover, it has been shown[9] that this universal behavior is not just an artifact of the μ^+SR method. Values of $\lambda_{ab}(0)$ obtained from magnetic torque and magnetization measurements for Y123 and $La_{2-x}Sr_xCuO_4$ (La214) also fall on the parabola.[9]

While the agreement of the data with Eq. (16) is good for underdoped, optimum doped, and mildly overdoped samples, there is evidence that this is not the case for heavily overdoped compounds. According to Eq. (16), overdoping the system should lead to an increasing $\sigma(0)$ and a decreasing T_c. However, in $Tl_2Ba_2CuO_{6+\delta}$ (Tl2201) (Refs. 15 and 16) and in $(YbCa)(BaSr)_2Cu_3O_{7-\delta}$ (Ca- and Sr-doped Yb123),[18] both $\sigma(0)$ and T_c decrease with overdoping. This behavior can be understood by taking into account the short-range repulsive interaction between the bosons.[63] Increasing the doping in the overdoped regime increases the boson density n_B. In this case, the short-range interaction causes the bosons to become more and more immobile (their effective mass m_B^* increases). As a consequence, T_c and the superfluid density $\rho(0) = n_B/m_B^* = n_s/4m_{ab}^* \propto \sigma(0)$ both decrease. The observed shape of $T_c(\sigma)$ over the whole doping regime then resembles the form of a fly wing. Nevertheless, the parabolic ansatz is consistent with experimental data of cuprate families lying in the underdoped and around the optimum doped region.

Equation (16) can be used to predict the T_c dependence of the pressure and the isotope coefficient yielding[7-9]

$$\alpha \simeq \alpha_m \pm 2\frac{\sqrt{1-\overline{T}_c}}{\overline{T}_c}\alpha_0, \quad \beta \simeq \beta_m \pm 2\frac{\sqrt{1-\overline{T}_c}}{\overline{T}_c}\beta_0 , \tag{17}$$

or

$$\alpha \simeq \alpha_m + \frac{1-\overline{\sigma}}{\overline{\sigma}(1-\overline{\sigma}/2)}\alpha_0, \quad \beta \simeq \beta_m + \frac{1-\overline{\sigma}}{\overline{\sigma}(1-\overline{\sigma}/2)}\beta_0 , \tag{18}$$

with

$$\alpha_m = \frac{1}{T_c^m}\frac{dT_c^m}{dp}, \quad \alpha_0 = \frac{1}{\sigma_m(0)}\frac{d\sigma(0)}{dp} , \tag{19}$$

and

$$\beta_m = -\frac{m}{T_c^m}\frac{dT_c^m}{dm}, \quad \beta_0 = -\frac{m}{\sigma_m(0)}\frac{d\sigma(0)}{dm} , \tag{20}$$

respectively. Here, $\alpha_0(\beta_0)$ is a constant specific to the material which may also depend on doping, and $\alpha_m(\beta_m)$ accounts for a small pressure (isotope mass) dependence of the optimally doped system. The signs + and − refer to $\sigma(0) < \sigma_m(0)$ and $\sigma(0) > \sigma_m(0)$, respectively. The μ^+SR depolarization rate can therefore be used to estimate the pressure and isotope coefficients, two crucial parameters required to understand the microscopic mechanisms responsible for high-T_c superconductivity. To test the prediction for the T_c dependence of the pressure coefficient α and the isotope coefficient β we applied Eq. (18) to our μ^+SR data of Y123, where $T_c^m \simeq 95$ K and $\sigma_m(0) \simeq 2.4$ μs^{-1}.[8] The estimated values of α and β thereby extracted are shown in Fig. 7 along with measured values of the pressure and isotope coefficients. Figure 7(a) shows $\alpha(\overline{T}_c)$ of the μ^+SR estimates (full circles). The solid line corresponds to Eq. (17) with $\alpha_m = 0.002$ kbar^{-1} and $\alpha_0 = 0.0037$ kbar^{-1}. The open symbols denote measurements of α by Bucher *et al.*[64] (triangles) and by Almasan *et al.*[65] (circles). The reasonable agreement between the measured values and the μ^+SR estimates is obvious, except for the two data points of Bucher *et al.* at $\overline{T}_c \simeq 0.675$ and $\overline{T}_c \simeq 0.78$, respectively. The reason for this deviation is not yet understood. Note that the universal behavior of the pressure coefficient is restricted to the $\overline{T}_c$-dependent part of Eq. (17), because α_0 is not expected to remain constant over the whole $\overline{T}_c$ range and α_0 as well as α_m may vary from family to family. In addition, Eq. (18) follows from the parabolic ansatz Eq. (16) which is only valid for a region not too far away from the optimal doping.

Figure 7(b) shows the μ^+SR estimates of $\beta(\overline{T}_c)$ for $(YPr)Ba_2Cu_3O_{6.97}$ [(YPr)123] (Ref. 66) (full circles). The curve corresponds to Eq. (17) with $\beta_m = 0.007$ and $\beta_0 = 0.113$. For comparison, the measured isotope coefficients of (YPr)123 from Ref. 67 (open circles) are also plotted. The experimental data are again consistent with the predicted behavior of $\beta(\overline{T}_c)$ given in Eq. (18). Interestingly, our μ^+SR estimates of $\beta(\overline{T}_c)$ for Y123 (full triangles) and measured values of β for $Y(BaLa)_2Cu_3O_{7-\delta}$ (Ref. 68) (open triangles) are also consistent with the behavior of β for (YPr)123. They show a similar trend in $\beta(\overline{T}_c)$ with the same parameters β_m and β_0. As for α_m and α_0, the same reservations concerning the universality of $\beta(\overline{T}_c)$ also apply for β_0 and β_m.

According to the results above, the data from μ^+SR and other measurements are in agreement with the predictions of the empirical ansatz Eq. (16) proposed in the framework of a Bose-gas picture. Moreover, this picture can also give an explanation for the varying shape of $\lambda_{ab}^{-2}(T)$ in the Y123 family presented in Sec. IV A. From

this viewpoint, a strongly underdoped system corresponds to a dilute Bose gas. Such a system is then well described by an ideal Bose gas with a temperature dependence of the penetration depth given by Eq. (13) with an exponent $n=3/2$. Increasing the carrier density up to optimal doping results in a system corresponding to a Bose gas in the dense limit. As shown by Weichman,[69] in this limit and for temperatures sufficiently far below T_c, an interacting critical region opens up where $\lambda(T)$ can be approximated by the two-fluid model ($n=4$).[9] As T becomes sufficiently close to T_c this will, however, cross over to a dependence given by $1/\lambda^2(T) = 1/\lambda^2(0)(1-T/T_c)^{2/3}$. The temperature dependence of λ in the *intermediate* temperature region thus depends on the boson density. The limiting cases of dilute and dense Bose gas should thus be well described by Eq. (13) using $n=3/2$ and $n=4$, respectively. The intermediate cases then follow from an interpolation between these two limits, which in a phenomenological way can be approximated by intermediate values of n. While, in principle, more exact interpolations could be made using the approach of Ref. 69, fits of Eq. (13) to the experimental data should yield values of n which qualitatively reflect the crossover from the dilute to the dense condensate limit.

The measurements of $\lambda_{ab}(T)$ of the Y123 family are indeed consistent with the above expectations: Samples in the underdoped regime exhibit a comparatively flat $\lambda_{ab}^{-2}(T)$, while samples near optimal doping show a two-fluid like behavior. This is shown in Fig. 8, where the exponent n which characterizes the overall temperature dependence of λ_{ab}^{-2} is plotted as a function of $\bar{\sigma}$. Unfortunately, the data presently available on the temperature dependence does not yet cover the region $0.5<\bar{\sigma}<1.1$ and in addition the exact form of $n(\bar{\sigma})$ is not known. The data points in the mildly overdoped region ($\bar{\sigma}>1$) suggest that the exponent n is probably larger than 4 for the optimal doping ($x\simeq 6.92$) and decreases by further doping in the heavily overdoped region. Indeed, it was proposed[70] that the exponent comes back to $n=3/2$ in the limit of maximum doping, where T_c and the superfluid density $\rho\propto\sigma$ vanish. As a consequence, $n(\bar{\sigma})$ would also exhibit a kind of a "fly wing" similar to that for $\bar{T}_c(\bar{\sigma})$.[63] It is interesting to note that Tl2201 (Ref. 15) seems to mimic this behavior, as shown in the inset of Fig. 8 (dashed line is a guide to the eye). However, the absolute values of the exponents are not in agreement with the expectations of the simple Bose-gas picture discussed above.

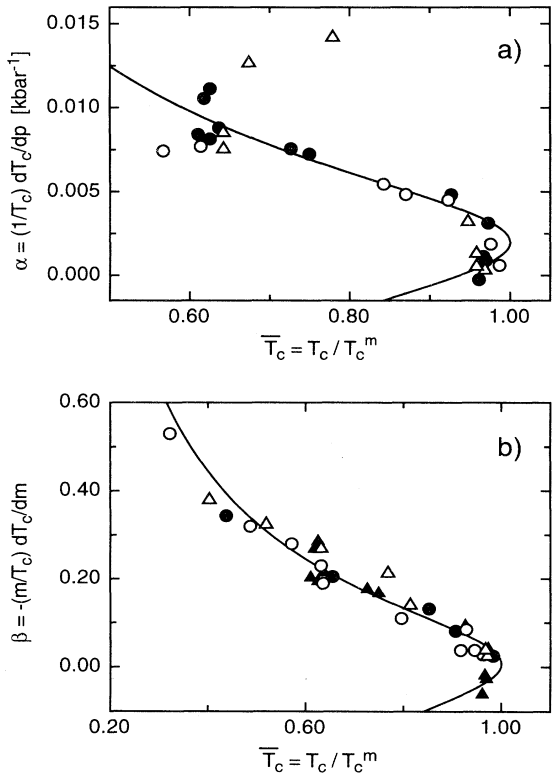

FIG. 7. Comparison of measured values of the pressure coefficient α and the isotope coefficient β as a function of the reduced transition temperature $\bar{T}_c=T_c/T_c^m$ with estimates from μ^+SR data:(a) $\alpha(\bar{T}_c)$ for $YBa_2Cu_3O_x$ (Y123) from Ref. 64 (open triangles) and Ref. 65 (open circles). The full circles denote estimates for α extracted from the μ^+SR data and Eq. (18) with $\alpha_m=0.002$ kbar^{-1} and $\alpha_0=0.0037$ kbar^{-1}. The solid line corresponds to Eq. (17) with the quoted values for α_m and α_0. (b) $\beta(\bar{T}_c)$ for Pr-doped Y123 [(YPr)123], from Ref. 67 (open circles). Full circles are μ^+SR estimates of β for (YPr)123 (Ref. 66) using Eq. (18) with $\beta_m=0.007$ and $\beta_0=0.113$. The solid line corresponds to Eq. (17) with the quoted values for β_m and β_0. Also included are estimates from our Y123 μ^+SR data using the same values for β_m and β_0 (full triangles) and measurements of β for $Y(BaLa)_2Cu_3O_7$ (Ref. 68) (open triangles).

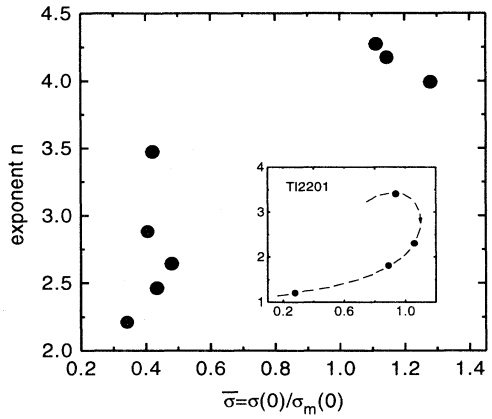

FIG. 8. Power-law exponent n [Eq. (13)] which characterizes the temperature dependence of $\lambda_{ab}^{-2}(T)$ as a function of $\bar{\sigma}=\sigma(0)/\sigma_m(0)$ of $YBa_2Cu_3O_x$. The data qualitatively follow the expectations of a Bose-gas picture, wherein the condensate density $\rho\propto\bar{\sigma}$. Increasing the doping from a highly underdoped system (small $\bar{\sigma}$) to an optimally doped one ($\bar{\sigma}=1$) corresponds to a crossover from a dilute to a dense Bose gas. This influences the form of the temperature dependence of $\lambda_{ab}^{-2}(T)$ such that n increases from 3/2 in the extreme-dilute limit (ideal Bose gas) to $n\approx 4$ in the dense limit. Inset shows $Tl_2Ba_2CuO_{6+\delta}$ data from Ref. 15: The exponent n is decreasing with increasing overdoping and follows the proposed behavior for the heavily overdoped regime, see text. The dashed line is a guide to the eye and the arrow indicates the direction of increasing oxygen content.

V. SUMMARY

In conclusion systematic μ^+SR experiments have been performed in order to investigate the temperature dependence of the magnetic penetration depth in terms of the measured depolarization rate in various samples of the Y123 family, as well as in Y124 and Bi2212. It is found that the behavior of $\lambda_{ab}(T)$ as extracted from $\sigma(T)$ is characteristic of each compound. This can be interpreted as a varying coupling strength in these systems. The form of $\sigma(T)$ is well described by the two-fluid model in Y123 with high oxygen content, indicating strong coupling with $2\Delta_0/k_B T_c \simeq 5$. The rest of the cuprates investigated show a $\sigma(T)$ which points to weaker coupling, with $\sigma(T)$ of highly oxygen-deficient Y123 being similar to the weak-coupling BCS prediction ($2\Delta_0/k_B T_c = 3.52$). In addition, the overall temperature dependence of σ varies in a systematic way with the oxygen stoichiometry x in the Y123 family. A further trend was also observed in the stoichiometry dependence of the low-temperature value of σ, which suggests a positive charge transfer into the CuO_2 planes with increasing x. The low-temperature values of the in-plane penetration depth $\lambda_{ab}(0)$ for all compounds measured range from 130(10) nm (Y123 with $x = 6.970$) to 255(20) nm (Y123 with $x = 6.546$) and are in good agreement with values found by other experimental methods.

In addition, our results are consistent with an empirical ansatz which has been proposed in the framework of a Bose-gas picture for high-T_c superconductivity. It is found that the data of λ_{ab} follow the predictions of this ansatz in (i), the relation between $\lambda_{ab}(0)$ and T_c (ii), the T_c dependence of the pressure and the isotope effect and in (iii), the doping dependence of the temperature behavior of λ_{ab}.

ACKNOWLEDGMENTS

We would like to thank T. Schneider for helpful discussions and also Dierk Herlach for technical support at PSI. This work was supported by the Swiss National Science Foundation (NFP30 No. 4030-32785) and by a special grant from the British-Swiss Joint Research Program.

*Author to whom correspondence should be addressed. Electronic address: lee@uzph3.physik.unizh.ch

[1]B. Batlogg, in *Physics of High-Temperature Superconductors,* edited by S. Maekawa and M. Sato, Springer Series in Solid-State Sciences, Vol. 106 (Springer-Verlag, Berlin, 1992), p. 219.

[2]S. I. Vedeneev *et al.*, Phys. Rev. B **49**, 9823 (1994); A. Plecenik *et al.*, *ibid.* **49**, 10016 (1994); A. M. Neminsky *et al.*, Phys. Rev. Lett. **72**, 3092 (1994); Ryozo Aoki, Hironaru Murakami, and Toshiyuki Kita, Physica C **225**, 1 (1994); V. A. Gasparov *et al.*, *ibid.* **231**, 197 (1994).

[3]See, e.g., Proceedings of the International Conference on Materials and Mechanisms of Superconductivity, High Temperature Superconductors III, Kanazawa, Japan [Physica C **185-189**, (1991)]; Proceedings of the International Conference on Materials and Mechanisms of Superconductivity, High Temperature Superconductors IV, Grenoble, France [Physica C **235-240** (1994)].

[4]Y. J. Uemura *et al.*, Phys. Rev. B **38**, 909 (1988).

[5]Y. J. Umeura *et al.*, Phys. Rev. Lett. **62**, 2317 (1989).

[6]Y. J. Uemura *et al.*, Phys. Rev. Lett. **66**, 2665 (1991).

[7]T. Schneider and H. Keller, Phys. Rev. Lett. **69**, 3374 (1992).

[8]T. Schneider and H. Keller, Physica C **207**, 366 (1993).

[9]T. Schneider and H. Keller, Int. J. Mod. Phys. B **8**, 487 (1994).

[10]D. R. Harshman *et al.*, Phys. Rev. B **47**, 2905 (1993).

[11]W. D. Wu *et al.*, Phys. Rev. B **47**, 8172 (1993).

[12]R. Cubitt *et al.*, Physica C **213**, 126 (1993).

[13]S. L. Lee *et al.*, Phys. Rev. Lett. **71**, 3862 (1993).

[14]M. Weber *et al.*, Phys. Rev. B **48**, 13 022 (1993).

[15]Ch. Niedermayer *et al.*, Phys. Rev. Lett. **71**, 1764 (1993).

[16]Y. J. Uemura *et al.*, Nature (London) **364**, 605 (1993).

[17]J. E. Sonier *et al.*, Phys. Rev. Lett. **72**, 744 (1994).

[18]C. Bernhard *et al.*, Physica C **226**, 250 (1994).

[19]B. Pümpin *et al.*, J. Less-Common Met. **164&165**, 994 (1990).

[20]B. Pümpin *et al.*, Hyperfine Interact. **63**, 25 (1990).

[21]H. Keller *et al.*, Physica C **185-189**, 1089 (1991).

[22]B. Pümpin, *et al.*, Phys. Rev. B **42**, 8019 (1990).

[23]See, e.g., A. Schenck, *Muon Spin Rotation Spectroscopy: Principles and Applications in Solid State Physics* (Hilger, Bristol, 1985).

[24]P. G. de Gennes, *Superconductivity of Metals and Alloys* (Benjamin, New York, 1966).

[25]E. H. Brandt, Phys. Rev. B **37**, 2349 (1988); J. Low Temp. Phys. **73**, 335 (1988).

[26]Yu.M. Belousov *et al.*, Sov. Phys. Usp. **33**, 911 (1990), and references therein.

[27]L. J. Campbell, M. M. Doria, and V. G. Kogan, Phys. Rev. B **38**, 2439 (1988).

[28]S. L. Thiemann, Z. Radović, and V. G. Kogan, Phys. Rev. B **39**, 2439 (1989).

[29]W. Barford and J. M. F. Gunn, Physica C **156**, 515 (1988).

[30]V. I. Fesenko, V. N. Gorbunov, and V. P. Smilga, Physica C **176**, 551 (1991).

[31]E. M. Forgan *et al.*, Nature (London) **343**, 735 (1990); R. Cubitt *et al.*, Nature (London) **365**, 407 (1993).

[32]G. J. Dolan *et al.*, Phys. Rev. Lett. **62**, 827 (1989); Phys. Rev. Lett. **62**, 2184 (1989); I. V. Grigorieva, J. W. Steeds, and K. Sasaki, Phys. Rev. B **48**, 16 865 (1993); Hongjie Dai, Jie Liu, and Charles M. Lieber, Phys. Rev. Lett. **72**, 748 (1994).

[33]D. S. Fisher, M. P. A. Fisher, and D. A. Huse, Phys. Rev. B **43**, 130 (1991); D. A. Huse, M. P. A. Fisher, and D. S. Fisher, Nature (London) **358**, 553 (1992).

[34]D. R. Harshman, A. T. Fiory, and R. J. Cava, Phys. Rev. Lett. **66**, 3313 (1991).

[35]E. H. Brandt, Phys. Rev. Lett. **66**, 3213 (1991).

[36]S. L. Lee *et al.* (unpublished).

[37]S. Rusiecki *et al.*, J. Less-Common Met. **164&165**, 31 (1990).

[38]J. Karpinski *et al.*, Nature (London) **336**, 660 (1988).

[39]K. Conder, S. Rusiecki, and E. Kaldis, Mat. Res. Bull. **24**, 581 (1989).

[40]H. Keller, IBM J. Res. Dev. **33**, 314 (1989).

[41]R. F. Kiefl *et al.*, Physica C **153-155**, 757 (1988).

[42]A. Schilling *et al.*, Phys. Rev. Lett. **71**, 1899 (1993).

[43]E. J. Ansaldo *et al.*, Physica C **185-189**, 1763 (1991).

[44]W. L. Lee and D. M. Ginsberg, Phys. Rev. B **45**, 7402 (1992).

[45]M. R. Schafroth, Phys. Rev. **100**, 463 (1955).

[46]B. Mühlschlegel, Z. Phys. **155**, 313 (1959).
[47]D. S. Reed *et al.*, Phys. Rev. B **49**, 4384 (1994).
[48]D. Zech (private communication).
[49]M. Yethiraj *et al.*, Phys. Rev. Lett. **70**, 857 (1993).
[50]D. A. Bonn *et al.*, Phys. Rev. B **47**, 11 314 (1993).
[51]E. J. Nicol and J. P. Carbotte, Phys. Rev. B **43**, 1158 (1991).
[52]J. Rammer, Europhys. Lett. **5**, 77 (1988).
[53]M. Prohammer and J. P. Carbotte, Phys. Rev. B **43**, 5370 (1991).
[54]C. Jiang and J. P. Carbotte, Phys. Rev. B **45**, 10 670 (1992).
[55]M. B. Reeves *et al.*, Phys. Rev. B **47**, 6065 (1993).
[56]A. M. Neminsky and P. N. Nikolaev, Physica C **212**, 389 (1993).
[57]B. Janossy *et al.*, Physica C **181**, 51 (1991).
[58]R. J. Cava *et al.*, Physica C **165**, 419 (1990).
[59]A. A. Aligia and J. Garcés, Phys. Rev. B **49**, 524 (1994).
[60]C. Martinez, Ph.D. thesis, University of Joseph Fourier Grenoble, 1991; D. Zech, diploma thesis, University of Zurich, 1991.
[61]B. G. Levi, Phys. Today **46**, 17 (1993), and references therein.
[62]R. J. Kelley *et al.*, Phys. Rev. Lett. **71**, 4051 (1993); T. P. Devereaux *et al.*, *ibid.* **72**, 396 (1994); P. Chaudhari and Shawn-Yu Lin, *ibid.* **72**, 1084 (1994); A. G. Sun *et al.*, *ibid.* **72**, 2267 (1994); J. Buan *et al.*, *ibid.* **72**, 2632 (1994); D. C. DeGroot *et al.*, Physica C **222**, 271 (1994); I. Iguchi and Z. Wen, Phys. Rev. B **49**, 12 388 (1994); C. C. Tsuei *et al.*, Phys. Rev. Lett. **73**, 593 (1994); M. Takigawa and D. B. Mitzi, *ibid.* **73**, 1287 (1994); D. A. Bonn *et al.*, Phys. Rev. B **50**, 4051 (1994); Ju Young Lee *et al.*, *ibid.* **50**, 3337 (1994); K. A. Moler *et al.*, Phys. Rev. Lett. **73**, 2744 (1994).
[63]T. Schneider, in *Proceedings of the Workshop on Polarons and Bipolarons in High-T_c Superconductors and Related Materials,* Cambridge, United Kingdom (Cambridge University Press, Cambridge, in press).
[64]B. Bucher *et al.*, *XIII AIRAPT Conference, Bangalore (India), 1991* (Oxford, New Delhi, 1992).
[65]C. C. Almasan *et al.*, Phys. Rev. Lett. **69**, 680 (1992).
[66]C. L. Seaman *et al.*, Phys. Rev. B **42**, 6801 (1990).
[67]J. P. Franck *et al.*, Physica C **172**, 90 (1990); Phys. Rev. B **44**, 5318 (1991).
[68]H. J. Bornemann and D. E. Morris, Phys. Rev. B **44**, 5322 (1991).
[69]P. Weichman *et al.*, Phys. Rev. B **38**, 8739 (1988).
[70]T. Schneider (private communication).